NASA TECHNICAL MEMORANDUM

NASA TM X- 62,350

NASA TM X-62,350

TEMPERATURE AND ELECTRICAL CONDUCTIVITY OF THE LUNAR INTERIOR FROM

MAGNETIC TRANSIENT MEASUREMENTS IN THE GEOMAGNETIC TAIL

Palmer Dyal
Ames Research Center
Moffett Field, Calif. 94035

Curtis W. Parkin
Department of Physics, University of Santa Clara
Santa Clara, Calif. 95053

William D. Daily
Department of Physics and Astronomy
Brigham Young University, Provo, Utah 84062

(NASA-TM-X-62350) TEMPERATURE AND
ELECTRICAL CONDUCTIVITY OF THE LUNAR
INTERIOR FROM MAGNETIC TRANSIENT
MEASUREMENTS IN THE GEOMAGNETIC TAIL
(NASA) 35 p HC CSCL 03B

N74-23376

G3/30 Unclas
39726

April 1974

Abstract---Magnetometers have been deployed at four Apollo sites on the moon to measure remanent and induced lunar magnetic fields. Measurements from this network of instruments have been used to calculate the electrical conductivity, temperature, magnetic permeability, and iron abundance of the lunar interior. Global lunar fields due to eddy currents, induced in the lunar interior by magnetic transients in the geomagnetic tail field, have been analyzed to calculate an electrical conductivity profile for the moon: the conductivity increases rapidly with depth from 10^{-9} mhos/meter at the lunar surface to 10^{-4} mhos/meter at 200 km depth, then less rapidly to 2×10^{-2} mhos/meter at 1000 km depth. This profile is generally consistent with conductivity results from transient response analysis in the solar wind, using data measured on the lunar nightside. A temperature profile is calculated from conductivity, using the data of Duba et al., (1972): temperature rises rapidly with depth to 1100°K at 200 km depth, then less rapidly to 1800°K at 1000 km depth. Recent magnetic permeability and iron abundance determinations are reported in a companion article (Parkin et al., 1974). Velocities and thicknesses of the earth's magnetopause and bow shock are estimated from simultaneous magnetometer measurements. Average speeds are determined to be about 50 km/sec for the magnetopause and 70 km/sec for the bow shock, although there are large variations in the measurements for any particular boundary crossing. Corresponding measured boundary thicknesses average to about 2300 km for the magnetopause and 1400 km for the bow shock.

INTRODUCTION

A network of three lunar surface magnetometers has been placed on the moon by astronauts during Apollo 12, 15, and 16 missions. Measurements of these surface magnetometers and lunar orbiting magnetometers have been used to investigate properties of the lunar crust and deep interior, including remanent lunar magnetic fields, their sources, and interactions with the solar wind plasma; magnetic permeability and iron abundance of the moon; and electrical conductivity and temperature of the lunar interior. Results of these investigations have recently been reviewed by Fuller (1974) and Dyal et al. (1974).

The electrical conductivity of the lunar interior, which is related to lunar temperature, has been investigated by analyzing the induction of global lunar fields by time-varying extralunar (solar or terrestrial) magnetic fields. When the moon is in the solar wind, lunar eddy current fields form an induced lunar magnetosphere which is distorted in a complex manner due to flow of solar wind plasma past the moon. The eddy current field is compressed on the dayside of the moon and is swept downstream and confined to the "cavity" on the lunar nightside. Because of the complexity of this asymmetric confinement of lunar fields by the solar wind, early analysis included a theory for transient response of a sphere in a vacuum in order to model lunar response as measured on the lunar nightside (Dyal and Parkin, 1971). Transient analysis has since evolved to include effects of cavity confinement on nightside tangential data and to introduce analysis of magnetic step transients measured on the lunar dayside (Dyal et al., 1973).

The asymmetric confinement of lunar fields is particularly complex to model theoretically (Schubert et al., 1973); indeed, the general time-dependent asymmetric induction problem has not been solved at the time of this writing. In order to circumvent this problem of asymmetry, we consider in this paper lunar eddy current response during times when the moon is in regions of the geomagnetic tail where plasma interaction effects encountered in the solar wind (asymmetric confinement, remanent field compression, plasma diamagnetism, etc.) are

minimal, and lunar response can be theoretically modeled by the response of a sphere in a vacuum.

From the electromagnetic response of the moon to magnetic field transients in the geomagnetic tail, we calculate an electrical conductivity profile which is then converted to temperature. We find that the new conductivity and temperature profiles are consistent with earlier analyses using data measured on the lunar nightside. Finally, we present the preliminary results of velocity and thickness measurements of the earth's magnetopause and bow shock, which have been estimated from simultaneous magnetometer measurements.

LUNAR MAGNETOMETERS AND THE LUNAR MAGNETIC ENVIRONMENT

The lunar magnetometers

A network of three lunar surface magnetometers has been placed on the moon by Apollo astronauts as shown in Fig. 1. The vector magnetic field has been measured three times per second and transmitted to earth from each of these three Apollo sites. Magnetometers in lunar orbit on board the Explorer 35 satellite (Sonett et al., 1967) and on Apollo 15 and 16 subsatellites (Coleman et al., 1972) measure the field external to the moon and transmit this information to earth. Also, portable magnetometers have been used by the astronauts at the Apollo 14 and 16 sites, to measure remanent fields at different locations along a surface traverse.

Each stationary lunar surface magnetometer (LSM) deployed at an Apollo site on the moon measures three orthogonal vector components of the lunar surface magnetic field using three fluxgate sensors (Gordon et al., 1965) located at the ends of three 100-cm-long orthogonal booms. The sensors are separated from each other by 150 cm and are 75 cm above the ground. The analog output of each sensor is internally processed by a low-pass digital filter and a telemetry encoder, and the output is transmitted to earth via the central station S-band transmitter. The magnetometer has two data samplers, the analog-to-digital converter (26.5 samples/second) and the central station telemetry encoder (3.3 samples/second). The prealias filter following the sensor electronics has attenuations of 3 dB at 1.7 Hz and 58 dB at the Nyquist frequency (13.2 Hz), with an attenuation rate of 22 dB/octave. The four-pole Bessel digital filter has an attenuation of 3 dB at 0.3 Hz and 48 dB at the telemetry sampling Nyquist frequency (1.6 Hz). Instrument resolution is 0.2γ. The instrument is also used as a gradiometer by sending commands to operate three motors in the instrument which rotate the sensors such that all simultaneously align parallel first to one of the boom axes, then to each of the other two boom axes in turn. This sensor alignment permits the vector gradient to be calculated in the plane of the sensors and also permits an independent measurement of the magnetic field vector at each sensor position. A detailed description of the stationary magnetometer is reported by Dyal et al. (1970).

The lunar portable magnetometer (LPM) was developed for astronaut deployment on the Apollo 14 and 16 missions. The instrument was designed to be a totally self-contained, portable experiment package. Three orthogonally oriented fluxgate sensors are mounted on the top of a tripod, positioned 75 cm above the the lunar surface. These sensors are connected by a 15-meter-long cable to an electronics box which contains a battery, electronics, and three field component readouts (meters on Apollo 14 LPM; digital displays on Apollo 16 LPM). The electronics box is mounted on the mobile equipment transporter for Apollo 14 and on the lunar roving vehicle for Apollo 16. Portable magnetometer measurements can be made only by manual activation by an astronaut. Instrument resolution is 1 γ or 2 γ for the Apollo 14 LPM and 0.2 γ for the Apollo 16 LPM. Instrument properties of the Apollo 16 LSM and LPM are listed in Table 1.

Table 1

Magnetic fields of the lunar environment are measured by the Explorer 35 satellite magnetometer. The satellite, launched in July 1967, has an orbital period of 11.5 hours, aposelene of 9390 km, and periselene of 2570 km (see Fig. 1 insert). The Explorer 35 Ames magnetometer measures three magnetic field vector components every 6.14 sec at 0.4 γ resolution; the instrument has an alias filter with 18 dB attenuation at the Nyquist frequency (0.08 Hz) of the spacecraft data sampling system. A more detailed description of the instrument is reported by Sonett et al. (1967).

The lunar magnetic environment

In different regions of a lunar orbit, the magnetic environment of the moon can have distinctly different characteristics (see Fig. 2). Average magnetic field conditions vary from relatively steady fields of magnitude ~ 9 in the geomagnetic tail to   turbulent fields averaging ~ 8 in the magnetosheath. Average solar wind velocity is ~ 400 km/sec in a direction approximately along the sun-earth line.

The interaction of the solar wind with the earth's permanent dipole field results in formation of the characteristic shape of the earth's magnetosphere; the solar wind in effect sweeps the earth's field back into a cylindrical region (the geomagnetic tail) on the earth's antisolar side. The earth's field magnitude is about 30,000 at the equator; in the geomagnetic tail the field decreases with distance from the earth with a radial dependence expressible as $R^{-0.736}$ (Mihalov et al., 1968). At the distance where the moon's orbit intersects the tail, the field magnitude is ~10 gammas. The moon is in the geomagnetic tail for about four days of each 29.5-day lunation (period between successive full moons). Substructure of the tail consists of two "lobes": the upper or northward lobe has its magnetic field pointing roughly toward the earth, whereas the lower lobe field points away from the earth. The moon can pass through either or both lobes, depending upon the characteristics of the particular orbit, the geomagnetic dipole axis orientation, and perturbations of the geomagnetic field by solar wind pressures.

LUNAR TEMPERATURE AND ELECTRICAL CONDUCTIVITY

Electrical conductivity and temperature of the moon have been
calculated from global eddy current response to changes in the magnetic field
external to the moon. When the moon is subjected to a change in the external
field, an eddy current field is induced in the moon which opposes the change
(see Fig. 3). The induced field responds with a time dependence which is a
function of the electrical conductivity distribution in the lunar interior. Simul-
taneous measurements of the transient driving field (by Explorer 35) and the
lunar response field (by an Apollo surface magnetometer) allow calculation of
the lunar conductivity. Since conductivity is related to temperature, a tempera-
ture profile can be calculated from an assumed compositional model of the
lunar interior.

. When the moon is in the solar wind, lunar eddy current fields form an
induced lunar magnetosphere which is distorted in a complex manner due to
flow of solar wind plasma past the moon. The eddy
current field is compressed on the dayside of the moon and is swept downstream
and asymmetrically confined to the "cavity" on the lunar nightside. Three-
dimensional, dynamic asymmetric confinement presents a difficult theoretical
problem which has not been solved at the time of this writing. Previous theoretical
approximations of the asymmetric problem have included a two-dimensional
approximation (Reisz et al. , 1972); three-dimensional static theory for a point-
dipole source, with substantiating laboratory data (Dyal and Parkin, 1973); a
three-dimensional "quasi-static" approach (Schubert et al. , 1973); and a three-
dimensional dynamic theory for one particular orientation of variations in the
external field (Schwartz and Schubert, 1973).

Because of the complexity of the asymmetric confinement problem, early
analysis included a theory for transient response of a sphere in a vacuum to
model lunar response in the solar wind, as measured on the lunar nightside.
In this paper time-dependent poloidal response of a sphere in a vacuum
has been applied to data measured in the geomagnetic tail where plasma confine-
ment effects are minimized, in order to determine electrical conductivity and
temperature profiles for the lunar interior.

In the following subsections response theory of a sphere in a vacuum is reviewed, after which the theory is applied to analyses of electrical conductivity, using lunar nightside data and geomagnetic tail data. Finally, we outline lunar temperature determinations from nightside and geomagnetic tail data.

Poloidal response of a sphere in a vacuum: theory

To describe the response of a lunar sphere to an arbitrary input field in the geomagnetic tail, we define the magnetic vector potential $\underline{A}$ such that $\nabla \times \underline{A} = \underline{B}$ and $\nabla \cdot \underline{A} = 0$. We seek the response to an input $\underline{\Delta B}_E b(t)$, where $b(t) = 0$ for $t < 0$ and $b(t)$ approaches unity as $t \rightarrow \infty$. (Since the governing equations are linear, the response to a more general input is readily found by superposition). The direction of $\underline{\Delta B}_E$ is taken to be the axis of a spherical coordinate system (r, θ, φ). If the conductivity is spherically symmetric, the transient magnetic field response has no ω component, and hence $A = Ae_\varphi$ and $\partial/\partial\omega = 0$. Under these conditions (and neglecting displacement currents) the laws of Faraday, Ampere, and Ohm combine to yield a diffusion equation (Dyal et al., 1972) for the magnetic potential (in MKS units):

$$\nabla^2 \underline{A} (r, \theta; t) = \mu \sigma (r) \frac{\partial \underline{A}}{\partial t} (r, \theta; t) \qquad (1)$$

We will show in a later section on magnetic permeability that we may take $\tilde{\mu} = \mu_o$ everywhere. Then, for $t > 0$, the magnetic field must be continuous at the surface, so that $\underline{A}$ and $\underline{A}/r$ must always be continuous at $r = R_m$, the radius of the sphere. We also have the boundary condition $A(0, t) = 0$ and the initial condition $\underline{A}(r, \theta, \varphi) = 0$ inside the moon. Outside the moon, where $\sigma = 0$,

$$A = \Delta B_E \left(\frac{r}{2}\right) b(t) \sin\theta + \frac{\Delta B_E}{r^2} f(t) \sin\theta . \qquad (2)$$

The first term on the right is a uniform magnetic field modulated by $b(t)$; the second term is the (as yet unknown) external transient response, which must vanish as r and $t \rightarrow \infty$. Note that at $r = R_m$, where R_m is normalized to unity,

$$A = \Delta B_E \sin\theta \left(\frac{b(t)}{2} + f(t)\right) \qquad (3)$$

and

$$\frac{\partial A}{\partial r} = \Delta B_E \sin\theta \left(\frac{b(t)}{2} - 2f(t)\right) . \qquad (4)$$

Therefore, at $r = R_m = 1$,

$$\frac{\partial A}{\partial r} = -2A + \frac{3}{2}\left(\Delta B_E \sin\theta \, b(t)\right) . \qquad (5)$$

Since the magnetic field is continuous at $r = R_m$, this is a boundary condition for the interior problem. Letting $G(r, t) = A/\Delta B_E \sin \theta$ and $\overline{G}(r, s)$ be the Laplace transform of G, equation (1) becomes

$$\frac{1}{r} \left(\frac{\partial^2}{\partial r^2} (r\overline{G}) - \frac{2}{r} \overline{G} \right) = s\mu_o \sigma(r)\overline{G} \tag{6}$$

for the interior. The boundary conditions are

$$\frac{\partial \overline{G}}{\partial r} = -2\overline{G} + \frac{3}{2} \overline{b}(s) \tag{7}$$

at $r = R_m$ and

$$\overline{G} = 0 \tag{8}$$

at $r = 0$.

For a given $\sigma(r)$ and $b(t)$, this system is numerically integrated to obtain $\overline{G}(r, s)$ in the range $0 \leq r \leq R_m$. The function $\overline{G}(r, s)$ is then numerically inverse Laplace transformed to find the characteristic transient response function $f(t)$ for the system. The resulting $f(t)$ is compared to the measurements and reiterated with a different function $\sigma(r)$ until the error between the calculated $f(t)$ and the measured $f(t)$ is minimized. The final $\sigma(r)$ is not unique; rather a family of $\sigma(r)$ is generated with the constraint that $f(t)$ match the experimental data.

Lunar nightside data analysis

The lunar electrical conductivity has been investigated by analysis of the
lunar response to transients in the solar wind magnetic field. The response,
measured by an Apollo magnetometer on the nightside of the moon, is theoretically
approximated by the response of a conducting sphere in a vacuum. The measured
response (illustrated in Fig. 4) is the average poloidal field response (for the radial
surface field component) to a normalized fast-ramp decrease in the external field.
Error bars are standard deviations of the measured responses. Chosen for the
analysis is a ramp input function which falls from unity to zero in 15 seconds, a
time characterizing convection of a solar wind discontinuity past the Moon. (For
a 400 km/sec solar wind, this time is 10-20 sec, depending on the thickness of
the discontinuity and the inclination of its normal to the solar wind velocity).

For a family of conductivity profiles, all of which monotonically increase
with depth in the moon, the theoretical response to a fast ramp is calculated and
compared to the measured response. A particular set of these conductivity
profiles yield response functions which pass within all data error bars of Fig. 4.
These profiles define the shaded region of Fig. 9 and are all consistent with the
nightside response data.

Conductivity results: geomagnetic tail data analysis.

Figs. 5 and 6 show examples of a magnetic transients measured in the geomagnetic tail. The data components are expressed in a coordinate system which has its origin on the lunar surface at the Apollo 12 magnetometer site. The x-component is directed radially outward from the lunar surface, while the y- and z-components are tangent to the surface, directed eastward and northward, respectively. The external (terrestrial) driving magnetic field is measured by Explorer 35, whereas the total response field is measured on the lunar surface by the Apollo 12 magnetometer.

To analyze these and similar events, the Explorer 35 input field components are fitted numerically by functions which are sums of ramp inputs chosen to fit the external field data. For a given conductivity model of the moon, the theoretical time series response to an external field data set is numerically calculated using the theory outlined in the previous section. This calculated response is then compared with the measured Apollo 12 time series data. Conductivity profiles have been constrained to be monotonically increasing with depth into the moon.

Fig. 7 shows an example of calculated response for the Explorer 35 x-axis (radial) input function of Fig. 5, using the electrical conductivity profile illustrated in Fig. 7 insert. Superimposed is the actual response, which is the Apollo 12 x-component of Fig. 5. Likewise, Fig. 8 shows calculated response for the radial components of Fig. 6, also using the conductivity profile shown in Fig. 7 insert. This conductivity profile yields the best fit of eighty profiles which have been run to date, although it is certainly not unique. The profile also yields theoretical responses which fit well for the measured tangential components of Figs. 5 and 6 and the components of twenty other geomagnetic tail transients which have been processed to date.

Fig. 9 summarizes electrical conductivity results from nightside and geomagnetic tail data, showing general agreement of the results. In the future many more geomagnetic transient events will be processed to determine a range of conductivity profiles consistent with a large data set.

Lunar temperature profiles from conductivity analyses

Once the electrical conductivity profile of the moon has been determined, an internal temperature distribution can be inferred for an assumed lunar material composition (see Rikitake, 1966). For cases where electrical conductivity is independent of pressure to a first approximation, the conductivity of materials can be expressed in terms of temperature T as follows:

$$\sigma = \sum_i E_i \exp(-a_i/kT) \qquad (9)$$

where a_i are the activation energies of impurity, intrinsic, and ionic modes, expressed in electron volts; E_i are material-dependent constants; and k is Boltzmann's constant. It should be emphasized that the electrical conductivity $\sigma(a, E, T)$ is a strong function of the material composition; therefore, uncertainties in knowledge of the exact composition of the sphere limits the accuracy of the internal-temperature calculation.

Laboratory results relating conductivity to temperature for various minerals, which are good geochemical candidates for the lunar interior, have been presented by many investigators (e. g. , England et al. , 1968; Schwerer et al. , 1972; Olhoeft et al. , 1973; Duba et al. , 1972; Duba and Ringwood, 1973). The recent work by Duba et al. (1972) on the electrical conductivity of olivine has been used to convert the electrical conductivity profiles of Fig. 9 to the temperature profiles shown in Fig. 10. Again we note the general agreement of temperature Fig. 10 profiles determined from vacuum response theory applied to magnetic data measured in the geomagnetic tail and nightside data measured with the moon in the solar wind.

PROPERTIES OF THE EARTH'S MAGNETOPAUSE AND BOW SHOCK

Using simultaneous data from magnetometers on the lunar surface and in orbit around the moon, the velocity and thickness of the earth's magneto-pause and bow shock (see Fig. 2) have been measured at the lunar orbit. Fig. 11 schematically shows the measurement technique. The boundary crossings are measured simultaneously by the Apollo 12 lunar surface magnetometer and the lunar orbiting Explorer 35 magnetometer (Fig. 12 shows an example of a magnetopause crossing). Assuming that the plane of a passing boundary layer is perpendicular to the solar ecliptic plane and that the boundary layer moves along its normal at the lunar orbit, the velocity of the layer is mea-sured from arrival-time difference measurements at the two instruments.

Elapsed-time data for shock and magnetopause motions as measured by magnetometers separated up to 10^4 km from each other, indicate that these boundaries are nearly always in motion and can have highly variable velocities. The magnetopause has an average speed of about 50 km/sec but measurements vary from less than 10 km/sec up to about 150 km/sec. Similarly, the bow shock has an average speed of about 70 km/sec but again there is a large spread in measured values from less than 10 km/sec to about 200 km/sec.

Based on the calculated boundary speeds and the signature of the boundary in the magnetometer data, thicknesses of the bow shock and magnetopause have been estimated. The average measured magnetopause thickness is about 2300 km; however, individual magnetopause boundaries range from 500 km to 5000 km in thickness. The average bow shock thickness is determined to be about 1400 km, with a spread in individual values ranging from 220 km to 3000 km.

SUMMARY

1. Lunar electrical conductivity and temperature

The electrical conductivity of the lunar interior has been investigated by analyzing the induction of global lunar fields by time varying extralunar (solar or terrestrial) magnetic fields. Analysis of lunar eddy current response to magnetic field transients in the solar wind, has yielded a conductivity profile rising from about 3×10^{-4} mhos/meter at 170 km depth in the moon to about 10^{-2} mhos/meter at 1000 km depth. In this paper electrical conductivity of the moon is determined from lunar eddy current response using magnetometer data measured during times when the moon is in the geomagnetic tail, in order to avoid the analytical problems posed by asymmetric solar wind confinement of the induced lunar magnetosphere. Preliminary results show that the following conductivity profile, though not unique, is generally consistent with input and response data: the conductivity increases rapidly with depth from 10^{-9} mhos/ meter at the surface to 10^{-4} mhos/meter at 200 km depth, then less rapidly to 2×10^{-2} mhos/meter at 1000 km depth. This profile falls within the error limits of the conductivity profile calculated from nightside data, as shown in Fig. 9.

The electrical conductivity determined from transient response in the geomagnetic tail is converted to a temperature profile using the data of Duba et al. (1972) for olivine. The temperature profile rises rapidly with depth from 270°K at the lunar surface to 1100°K at 200 km depth, then less rapidly to 1800°K at 1000 km depth.

2. Velocity and thickness of the earth's magnetopause and bow shock

Velocities and thicknesses of the earth's magnetopause and bow shock have been estimated from simultaneous magnetometer measurements. Average speeds are about 50 km/sec for the magnetopause and about 70 km/sec for the bow shock, with large spreads in individual measured values. Average thicknesses are about 2300 km for the magnetopause and 1400 km for the bow shock, also with large spreads in individual measured values.

REFERENCES

Coleman P. J. Jr., Lichtenstein B. R., Russell C. T., Schubert G., and Sharp L. R. (1973) The particles and fields subsatellite magnetometer experiment. In Apollo 16 Preliminary Science Report, NASA SP-315, pp. 23-1 to 23-13.

Duba A., and Ringwood A. E., Electrical conductivity, internal temperatures and thermal evolution of the moon, The Moon, 7, 356, 1973.

Duba A., Heard H. C., and Schock R. N., The lunar temperature profile, Earth Planet. Sci. Letters, 15, 301, 1972.

Dyal P. and Parkin C. W. (1971) The Apollo 12 magnetometer experiment: Internal lunar properties from transient and steady magnetic field measurements. Proc. Second Lunar Sci. Conf., Geochim. Cosmochim. Acta, Suppl. 2, Vol. 3, pp. 2391-2413. MIT Press.

Dyal P. and Parkin C. W. (1973) Global electromagnetic induction in the moon and planets. Phys. Earth Planet. Interiors, 7, 251-265.

Dyal P., Parkin C. W., and Sonett C. P. (1970) Lunar surface magnetometer, IEEE Trans. on Geoscience Electronics GE-8(4), 203-215.

Dyal P., Parkin C. W., and Cassen P. (1972) Surface magnetometer experiments: Internal lunar properties and lunar surface interactions with the solar plasma. Proc. Third Lunar Sci. Conf., Geochim. Cosmochim. Acta, Suppl. 3, Vol. 3, pp. 2287-2307. MIT Press.

Dyal P., Parkin C. W., and Daily W. D., Surface magnetometer experiments: Internal lunar properties, Proc. Fourth Lunar Science Conf., Geochim. Cosmochim. Acta, Suppl. 4, edited by W. A. Gose, Vol. 3, pp. 2229-2945, Pergamon, 1973.

Dyal P., Parkin C. W., and Daily W. D., Magnetism and the interior of the moon, submitted to Rev. Geophys. Space Phys., 1974.

England A. W., Simmons G., and Strangway D., Electrical conductivity of the moon, J. Geophys, Res., 73, 3219, 1968.

Fuller M., Lunar magnetism, Rev. Geophys. Space Phys., in press, 1974.

Gordon D. I., Lundsten, R. H., and Chiarodo R. A., Factors affecting the sensitivity of gamma-level ring-core magnetometers, IEEE Trans. on Magnetics, MAG-1(4), 330, 1965.

Mihalov J. D., Colburn D. S., Currie R. G., and Sonett C. P., Configuration and reconnection of the geomagnetic tail, J. Geophys. Res. 73, 943, 1968.

Olhoeft G. R., Frisillo A. L., Strangway D. W., and Sharpe H., Electrical properties of lunar solid samples, in Lunar Science IV, edited by J. Chamberlain and C. Watkins, The Lunar Science Institute, Houston, pp. 575-577, 1973.

Parkin C. W., Daily W. D., and Dyal P. (1974) Iron abundance and magnetic permeability of the moon. Submitted to Proc. Fifth Lunar Sci. Conf. Geochim. Cosmochim Acta, Suppl. 5, Vol. 3.

Reisz A. C., Paul D. L., and Madden T. R. (1972) The effects of boundary condition asymmetries on the interplanetary magnetic field-moon interaction. The Moon 4, 132-140.

Rikitake T., Electromagnetism and the Earth's Interior, Elsevier, Amsterdam, 1966.

Schubert G., Sonett C. P., Schwartz K., and Lee H. J., Induced magnetosphere of the moon 1. Theory, J. Geophys. Res., 78, 2094-2110, 1973.

Schwartz K., and Schubert G., Lunar electromagnetic scattering I. Propagation parallel to the diamagnetic cavity axis, J. Geophys. Res., 78, 6496-6506, 1973.

Schwerer F. C., Huffman G. P., Fisher R. M., and Nagata T., D. C. electrical conductivity of lunar surface rocks, The Moon, 4, 187, 1972.

Sonett C. P., Colburn D. S., Currie R. G., and Mihalov J. D. (1967) The geomagnetic tail; topology, reconnection and interaction with the moon. In Physics of the Magnetosphere (editors R. L. Carovillano, J. F. McClay, and H. R. Radoski). D. Reidel.

Table 1. Apollo surface magnetometer characteristics.

Parameter	Apollo 16 stationary magnetometer (LSM)	Apollo 16 portable magnetometer (LPM)
Ranges, gammas (each sensor)	0 to $\pm$ 200 0 to $\pm$ 100 0 to $\pm$ 50	0 to $\pm$ 256
Resolution, gammas	0.1	0.1
Frequency response, Hz	dc to 3	dc to 0.05
Angular response	Cosine of angle between field and sensor	Cosine of angle between field and sensor
Sensor geometry	3 orthogonal sensors at ends of 100 cm booms	3 orthogonal sensors in 6 cm cube
Analog zero determination	180° flip of sensor	180° flip of sensor
Power, watts	3.5	1.5 (battery)
Weight, kg	8.9	4.6
Size, cm	63x28x25	56x15x14
Operating temperature $^{\circ}$C	-50 to + 85	0 to +50
Commands	10 ground; 1 spacecraft	

FIGURE CAPTIONS

Fig. 1. Apollo magnetometer locations and measurements on the lunar surface.
Maximum remanent magnetic fields measured at each landing site are
shown. The insert shows an orbit of the Explorer 35 spacecraft, pro-
jected onto the solar ecliptic plane.

Fig. 2. Magnetic environment of the moon during a lunar orbit, with emphasis
on the geomagnetic tail region. The earth's permanent dipole field is
swept back into a cylindrical region known as the geomagnetic tail; at
the lunar distance the field magnitude is ~ 10 gammas $(10^{-4}$ gauss).
Substructure of the tail includes two lobes which are separated by the
neutral sheet current boundary; the upper or northward lobe has its
magnetic field (dark arrow) pointing roughly toward the earth, where-
as the southward lobe field points away from the earth.

Fig. 3. Global eddy current induction with the Moon in the geomagnetic tail.
The induced poloidal field is considered to be in a vacuum in the deep-
lobe regions of the tail.

Fig. 4. Lunar transient response data, measured by the Apollo 12 surface mag-
netometer while on the nightside, when the moon is in the solar wind.
The nightside transient response data, show decay characteristics of
the radial component of the total surface field B_{Ax} after arrival of a
step transient which reduces the external magnetic field radial compo-
nent by an amount ΔB_{Ex}, here normalized to one. The shape of the
curve illustrates time characteristics of the time decay of the induced
poloidal eddy-current field.

Fig. 5. Transient event in the geomagnetic tail, measured simultaneously by
the Apollo 12 LSM and the Explorer 35 Ames magnetometer. Data are
expressed in the surface coordinate system which has its origin at the
Apollo 12 magnetometer site; $\hat{x}$ is directed radially outward from the
surface, while $\hat{y}$ and $\hat{z}$ are tangent to the surface, directed eastward
and northward, respectively. Due to poloidal field induction in the
moon, the Apollo 12 radial $(\hat{x})$ component is "damped" relative to the
Explorer 35 radial component, whereas the Apollo 12 tangential $(\hat{y}$ and
$\hat{z})$ field components are "amplified" relative to Explorer 35 data.

Apollo 12 and Explorer 35 component data scales differ due to the existence of a $38 \overset{+}{-} 3$ gamma remanent field at the Apollo 12 surface site.

Fig. 6. Another transient event, measured deep in the northward lobe of the geomagnetic tail. Details concerning the data are given in Fig. 5 caption.

Fig. 7. Electrical conductivity analysis for a transient event in the geomagnetic tail. Shown are data from the radial component of the event of Fig. 5. Response to the Explorer 35 external field radial component is computed numerically for the conductivity profile shown in the insert and compared to the measured Apollo 12 response field. In the preliminary results of geomagnetic tail conductivity analysis, this selected conductivity profile, though not unique, yields a satisfactory fit of input and response data for this and twenty other tail events processed to date.

Fig. 8. Electrical conductivity analysis for another transient event measured deep in the northward lobe of the geomagnetic tail. Shown are data from the radial component of the event of Fig. 6. Response to the Explorer 35 external field radial component is computed numerically for the conductivity profile shown in the Fig. 7 insert and compared to the measured Apollo 12 response field.

Fig. 9. Electrical conductivity profile for the lunar interior calculated from measurements in different regions of the lunar orbit around the earth. The shaded region is from nightside transient analysis in the solar wind. The solid curve is from transient analysis in the geomagnetic tail.

Fig. 10. Temperature profile of the lunar interior, determined from the conductivity profile in Fig. 9. A lunar interior composition of olivine is assumed; laboratory data for olivine from Duba et al. (1972) are used in the calculation.

Fig. 11. Schematic diagram depicting a crossing of the magnetosphere boundary layer (the magnetopause) past the moon. Velocity of the layer is determined by using arrival-time difference measurements at the two instruments along with known distances between the instruments along

the direction of travel of the magnetopause.

Fig. 12. Magnetopause crossing, measured by the Apollo 12 lunar surface magnetometer and the lunar orbiting Ames Explorer 35 magnetometer. Data are expressed in the lunar surface coordinate system which has its origin at the Apollo 12 magnetometer site; $\hat{x}$ is directed radially outward from the surface, while $\hat{y}$ and $\hat{z}$ are tangent to the surface, directed eastward and northward, respectively. Shaded regions show arrival-times at the two instruments.
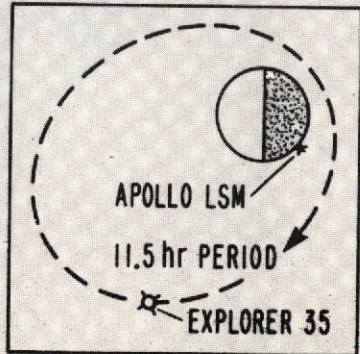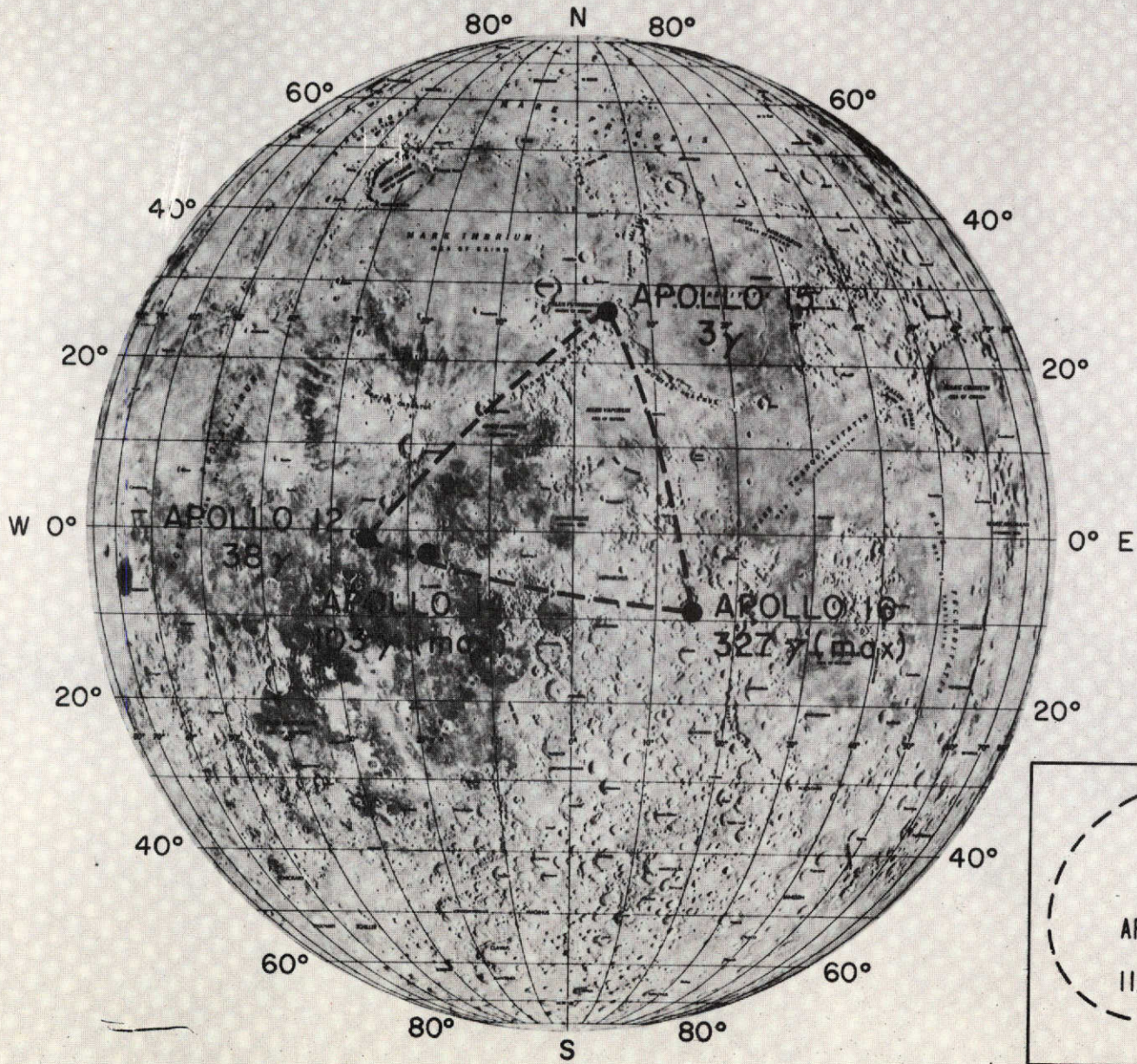
Fig. 1
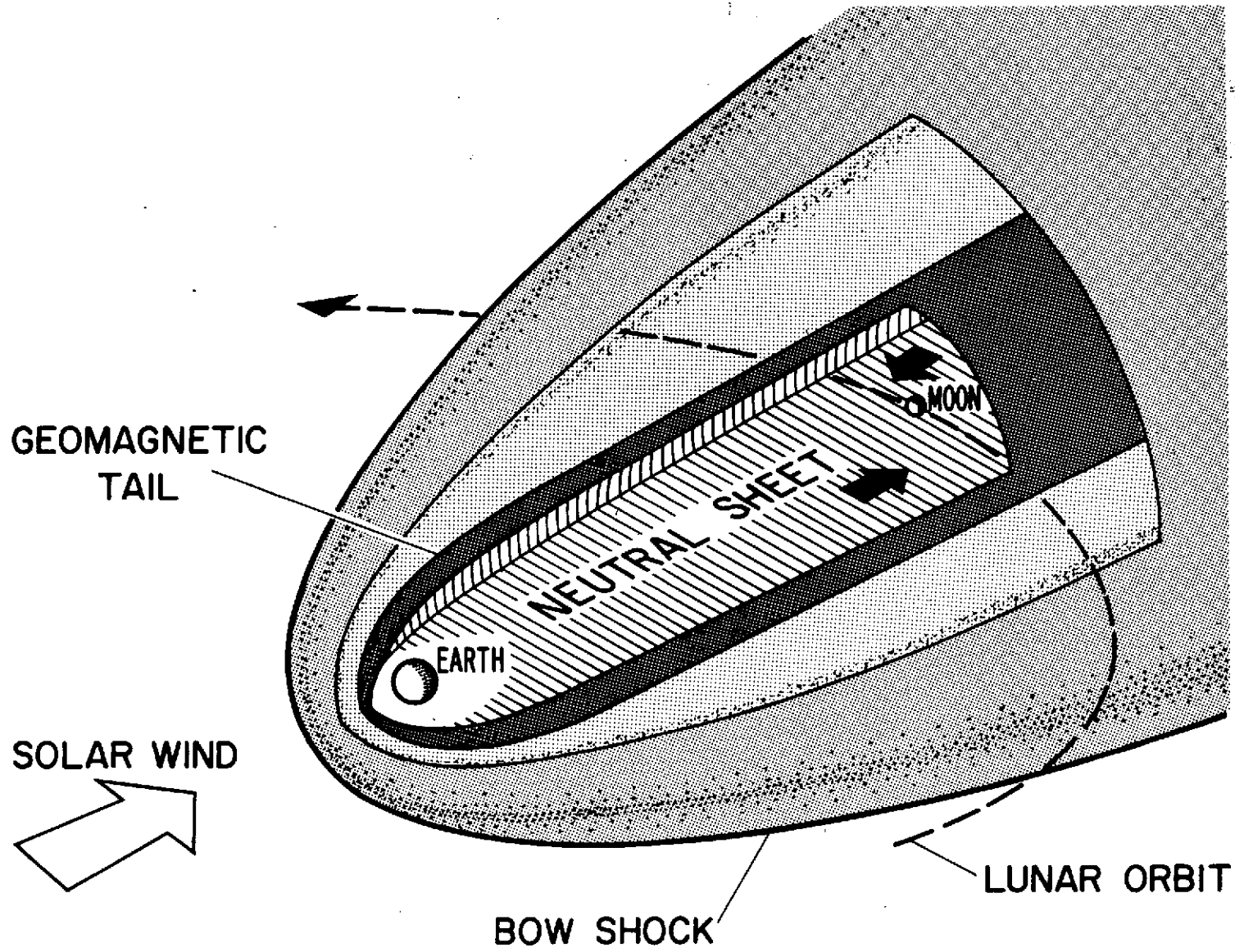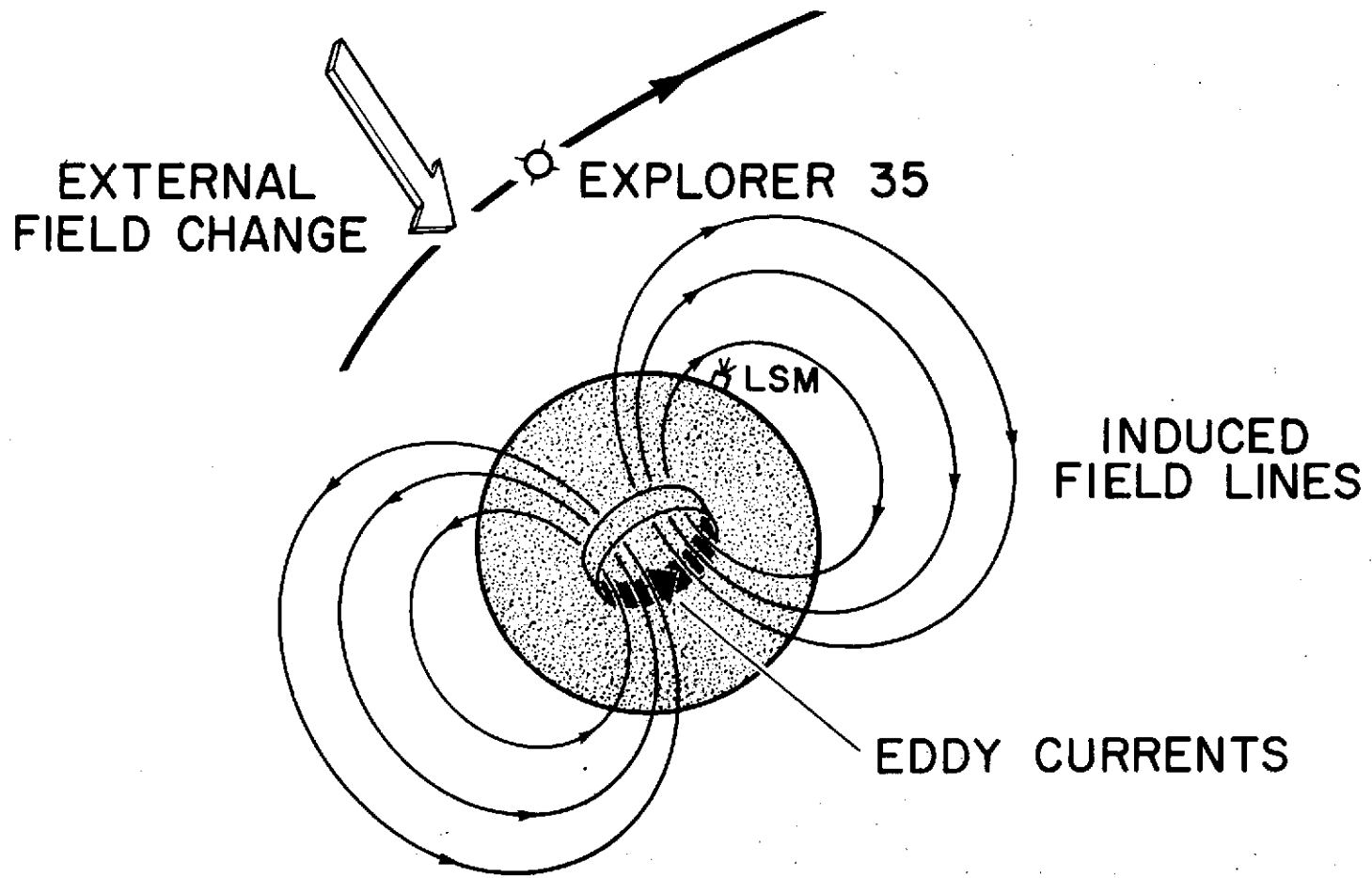
GEOMAGNETIC TAIL

SOLAR WIND

NEUTRAL SHEET

MOON

EARTH

LUNAR ORBIT

BOW SHOCK

Fig. 2

EXTERNAL
FIELD CHANGE

EXPLORER 35

LSM

INDUCED
FIELD LINES

EDDY CURRENTS

Fig. 3
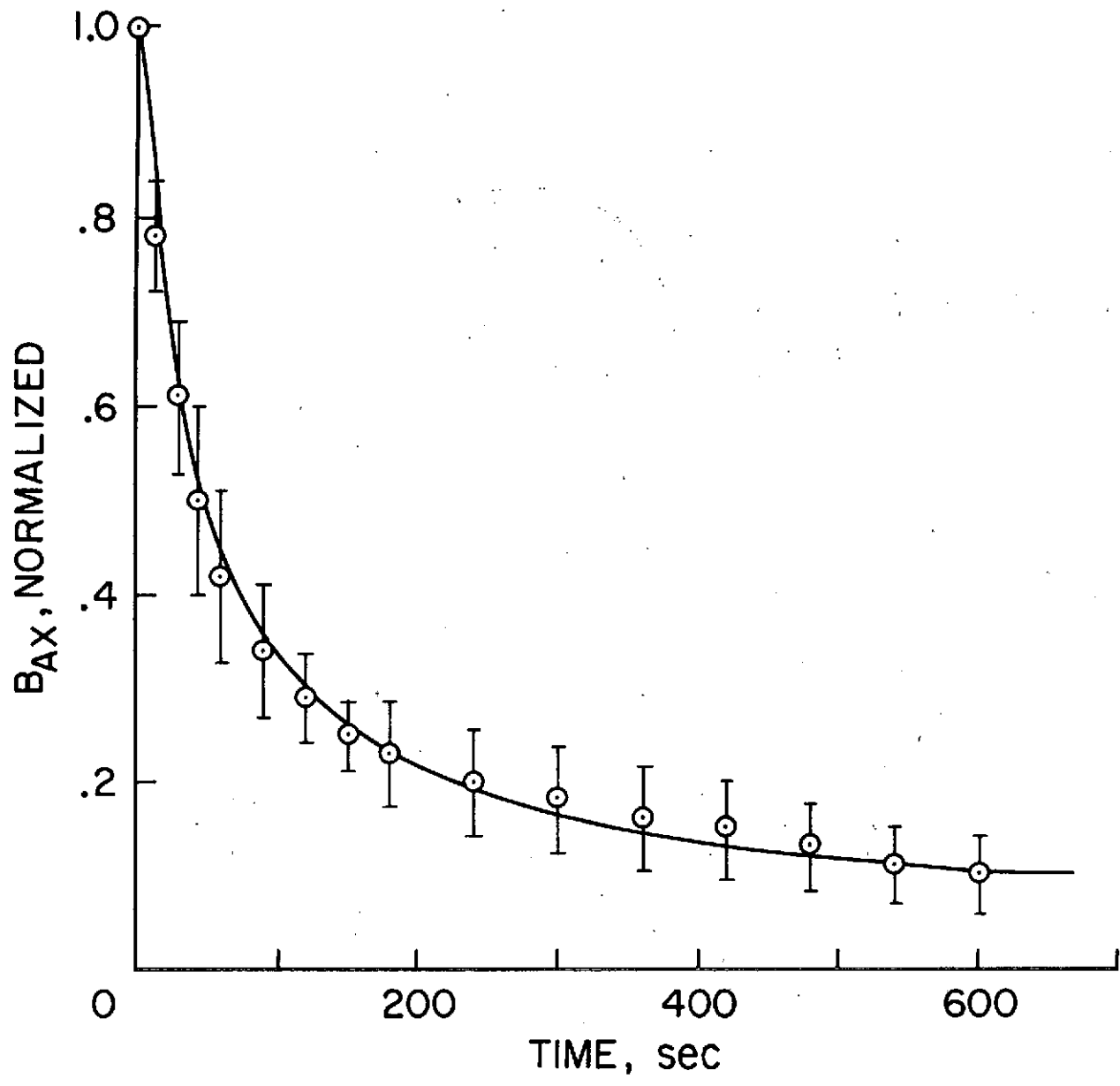
Fig. 4

GEOMAGNETIC TAIL TRANSIENT RESPONSE
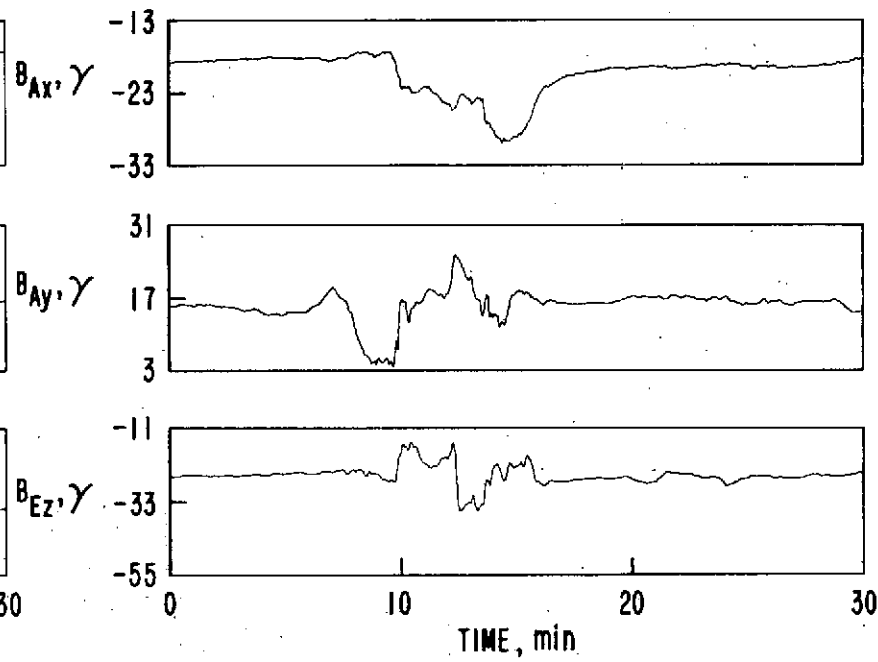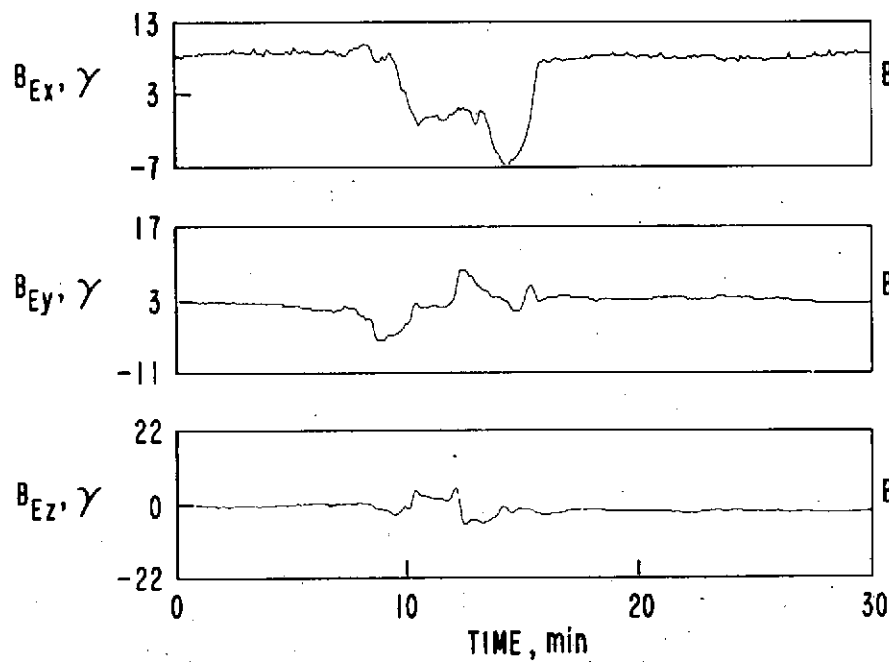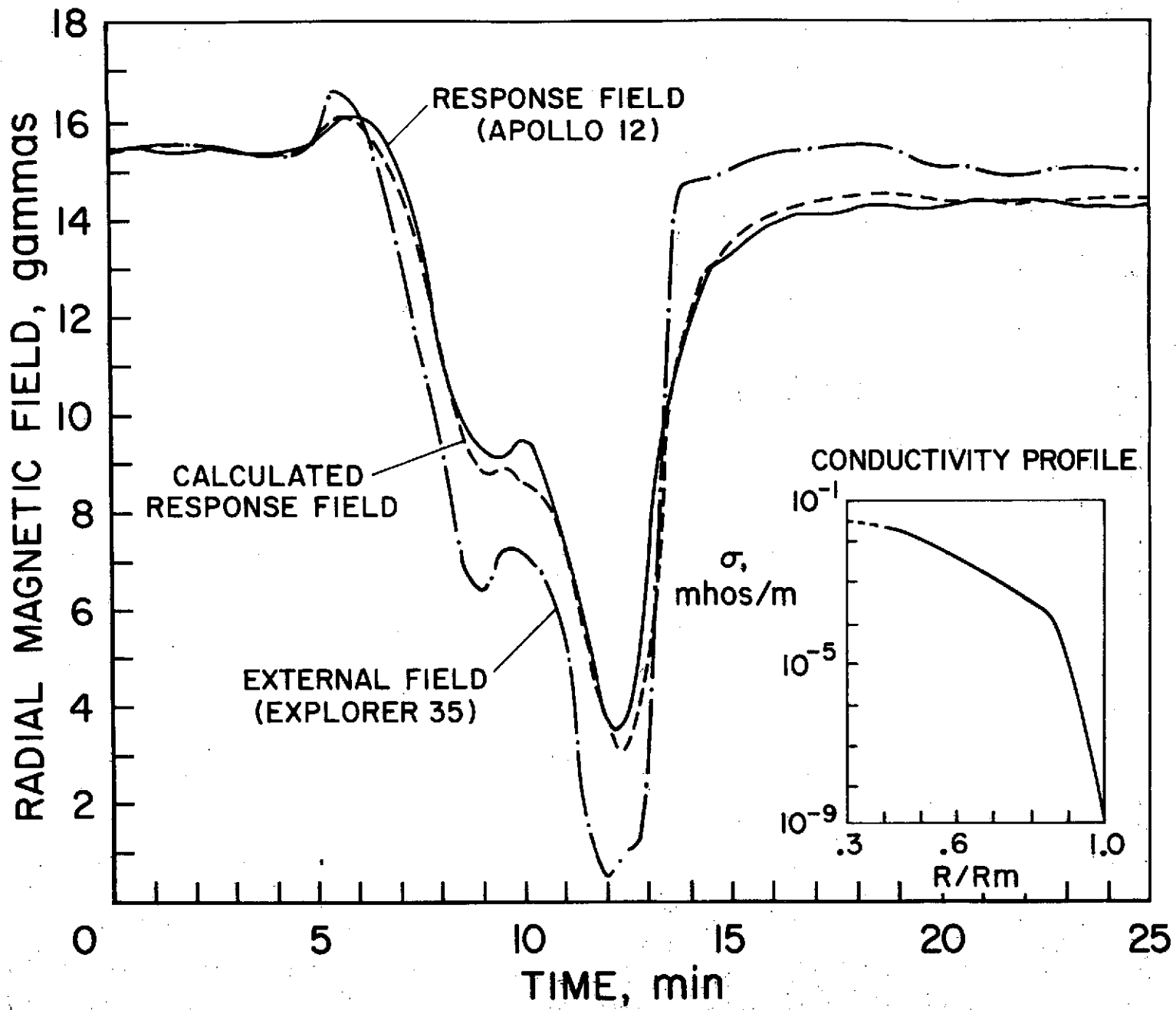

Fig. 5

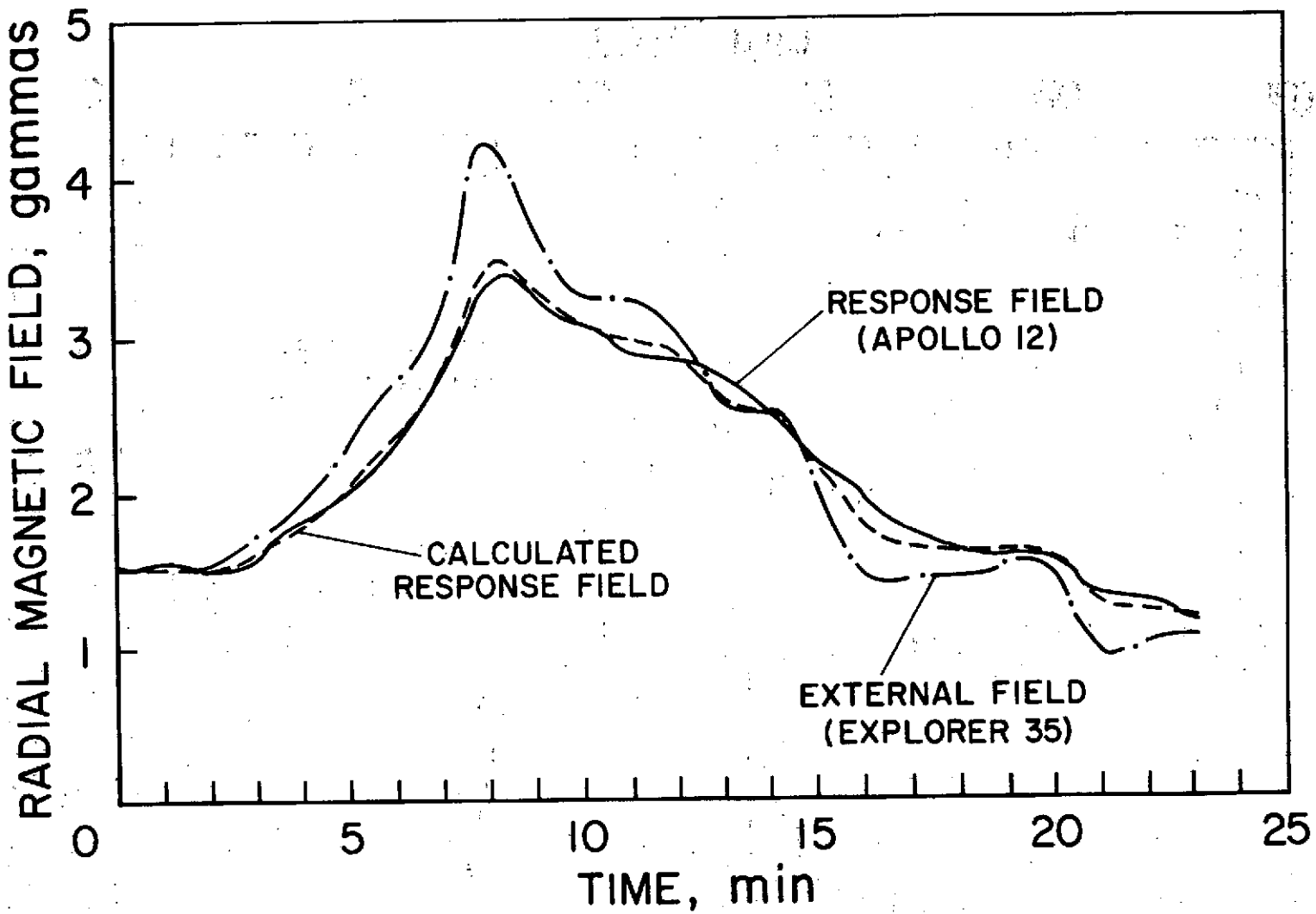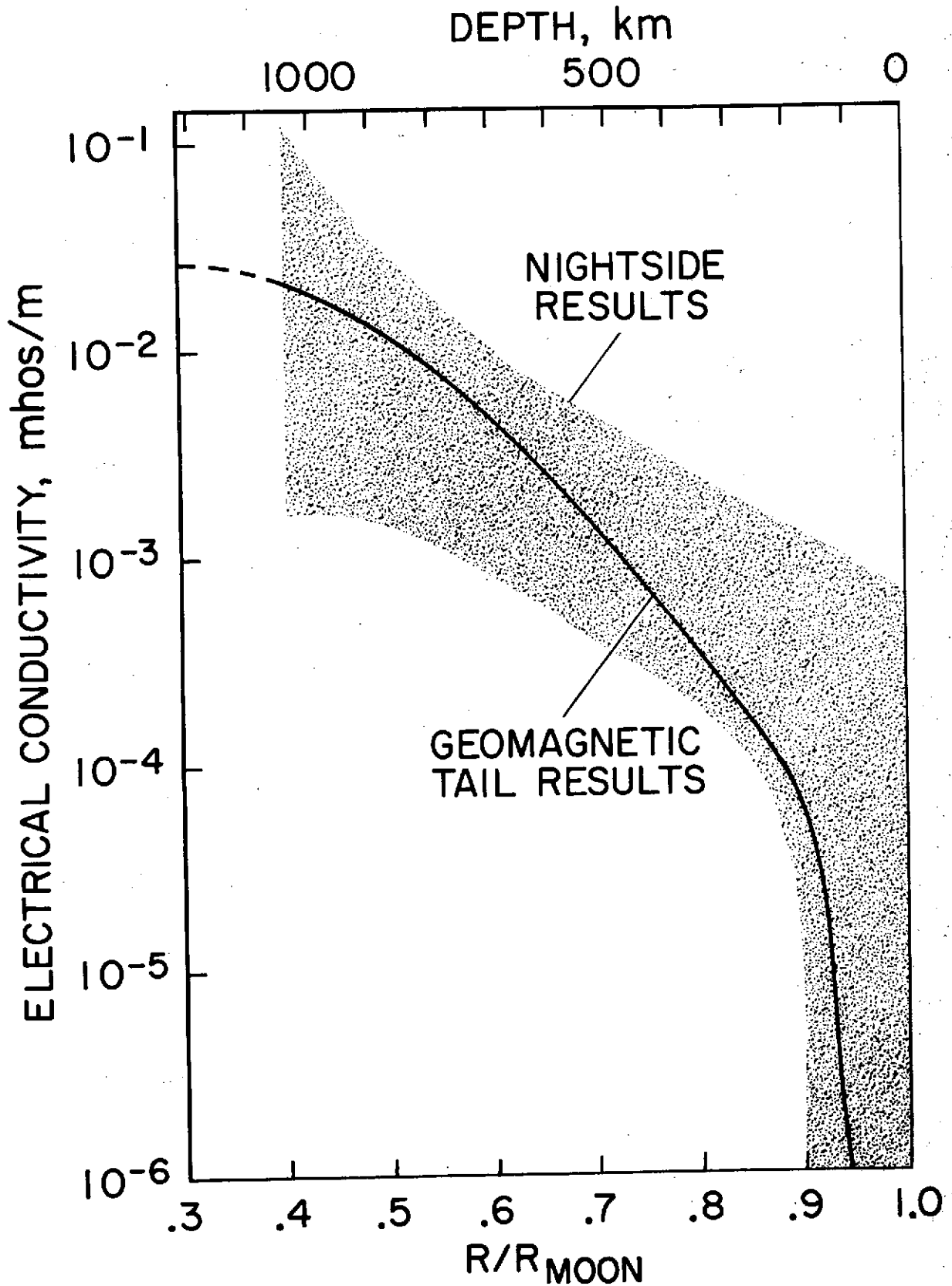# GEOMAGNETIC TAIL TRANSIENT RESPONSE
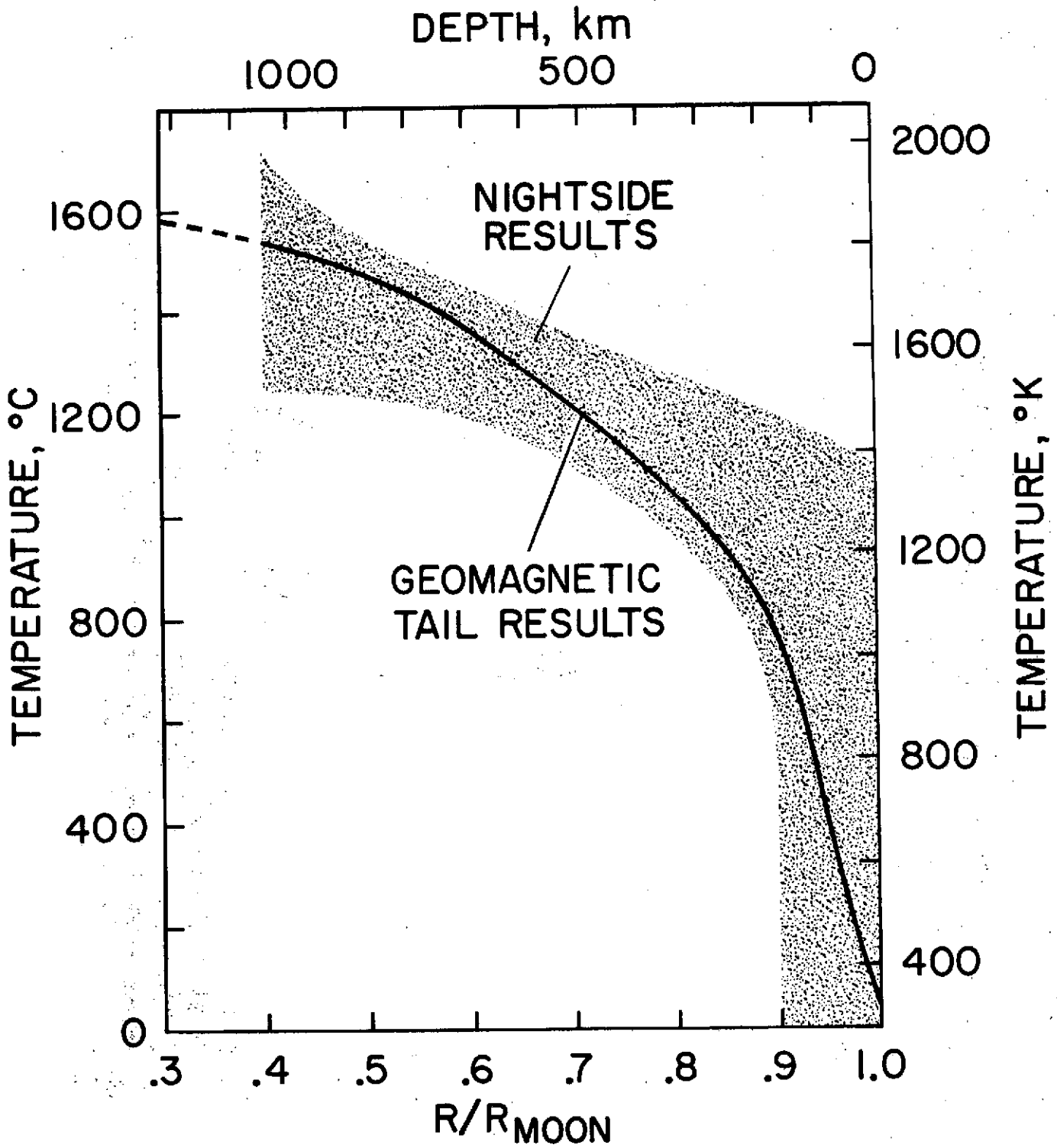

Fig. 6

Fig. 7

Fig. 8

-30-
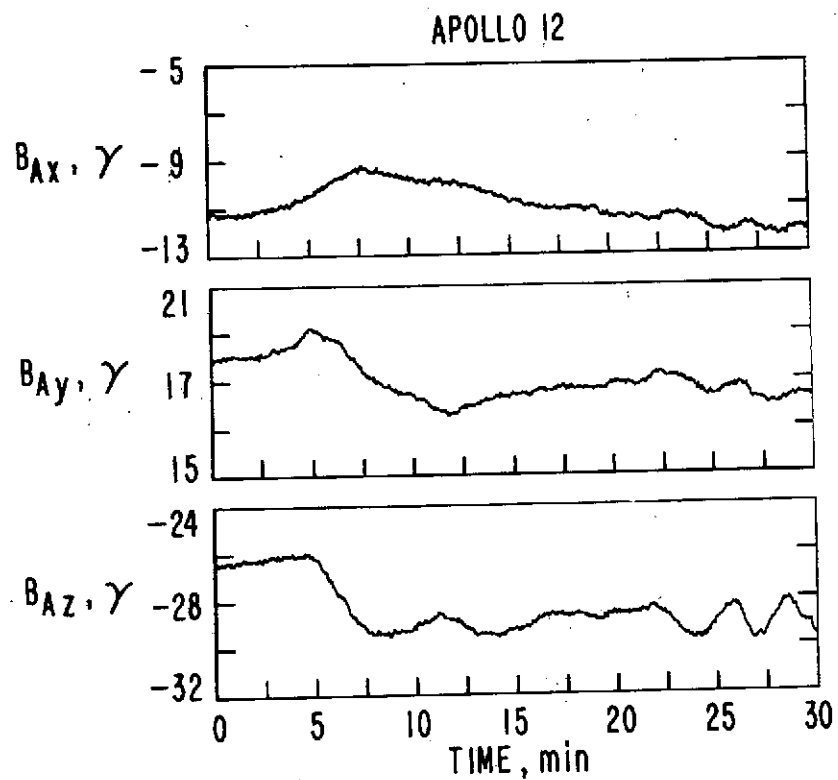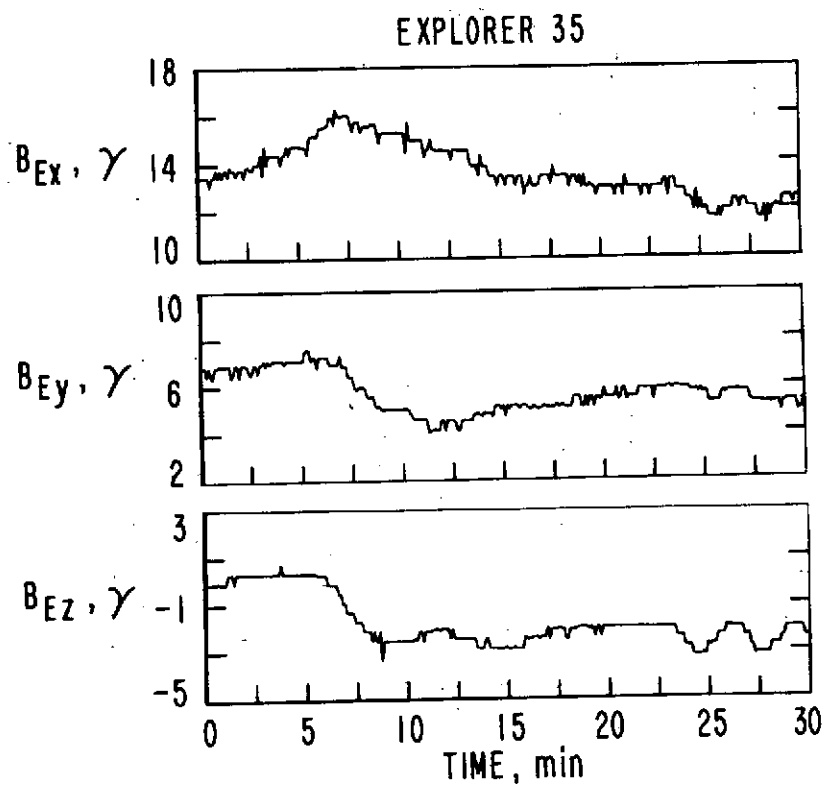
LUNAR CONDUCTIVITY PROFILE

Fig. 9

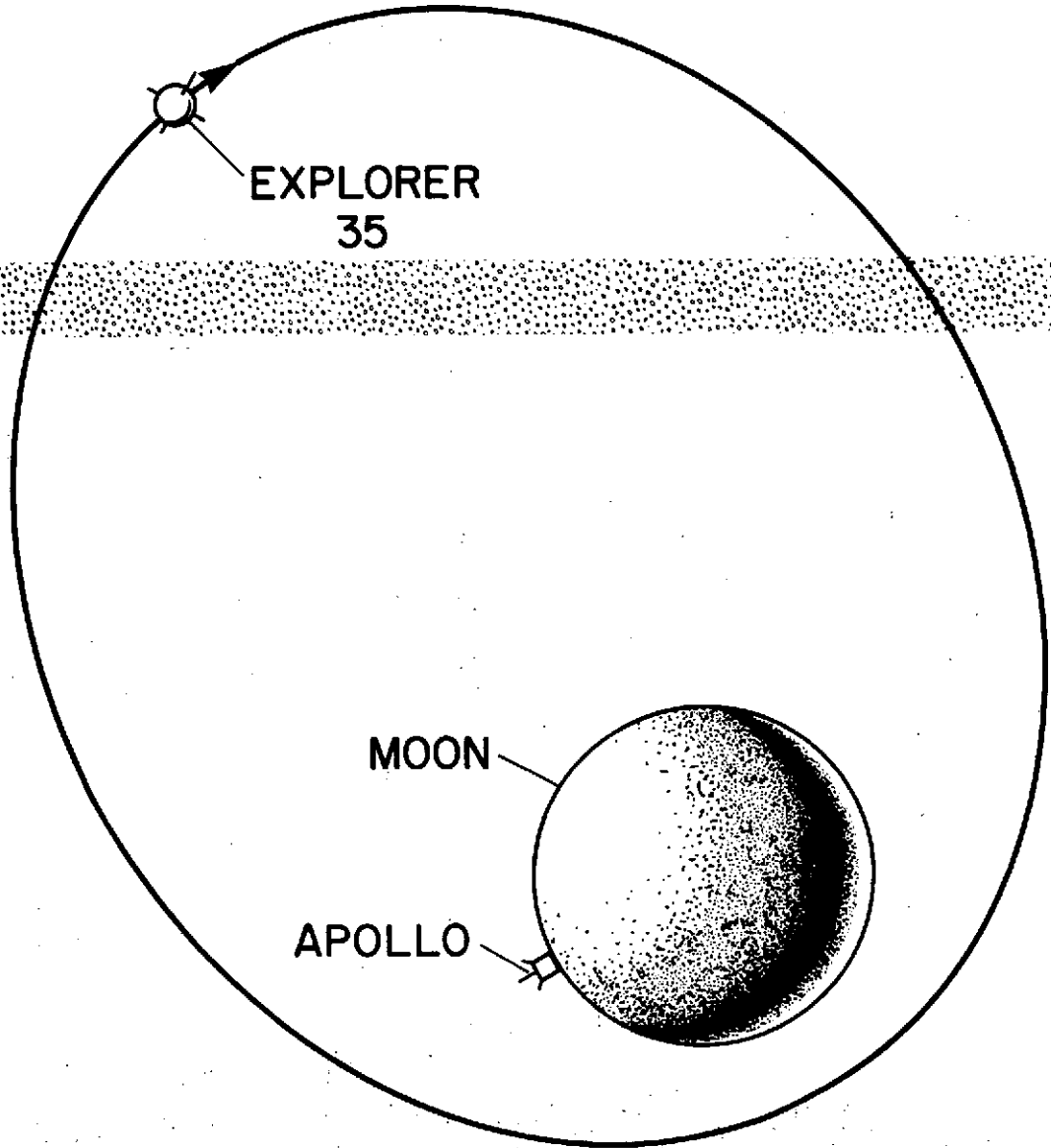LUNAR TEMPERATURE PROFILE
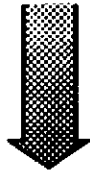
MAGNETOSHEATH

MAGNETOPAUSE

GEOMAGNETIC
TAIL

EXPLORER
35

MOON

APOLLO

TO
SUN

TO
EARTH

-33-

MAGNETOPAUSE CROSSING

EXPLORER 35
MAGNETOMETER

B_X, γ

B_Y, γ

B_Z, γ

APOLLO 12
MAGNETOMETER

B_X, γ

B_Y, γ

B_Z, γ

START: YEAR 1970
83D 15H 35M

TIME (min)

Fig. 12